Bioactive Materials 43 (2025) 319–329

Contents lists available at ScienceDirect

Bioactive Materials

journal homepage: www.keaipublishing.com/en/journals/bioactive-materials

Engineered endothelium-mimicking antithrombotic surfaces via combination of nitric oxide-generation with fibrinolysis strategies

Wenxuan Wang [a], Qing Ma [a,b], Da Li [a], Wentai Zhang [b], Zhilu Yang [b,***], Wenjie Tian [c,**], Nan Huang [a,d,*]

[a] School of Materials Science and Engineering, Key Lab of Advanced Technology of Materials of Education Ministry, Southwest Jiaotong University, Chengdu, 610031, China
[b] Dongguan Key Laboratory of Smart Biomaterials and Regenerative Medicine, The Tenth Affiliated Hospital of Southern Medical University, Dongguan, Guangdong, 523059, China
[c] Cardiology Department, Sichuan Provincial People's Hospital, University of Electronic Science and Technology of China, Chengdu, Sichuan 610072, China
[d] GuangZhou Nanchuang Mount Everest Company for Medical Science and Technology, Guangzhou, Guangdong, 510670, China

ARTICLE INFO

Keywords:
Nitric oxide
Fibrinolysis
Endothelium mimicking
Antithrombosis
Surface modification

ABSTRACT

Thrombosis associated with implants can severely impact therapeutic outcomes and lead to increased morbidity and mortality. Thus, developing blood-contacting materials with superior anticoagulant properties is essential to prevent and mitigate device-related thrombosis. Herein, we propose a novel single-molecule multi-functional strategy for creating blood-compatible surfaces. The synthesized azide-modified Cu-DOTA-$(Lys)_3$ molecule, which possesses both NO release and fibrinolysis functions, was immobilized on material surfaces via click chemistry. Due to the specificity, rapidity, and completeness of click chemistry, the firmly grafted Cu-DOTA-$(Lys)_3$ endows the modified material with excellent antithrombotic properties of vascular endothelium and thrombolytic properties of fibrinolytic system. This surface effectively prevented thrombus formation in both *in vitro* and *in vivo* experiments, owing to the synergistic effect of anticoagulation and thrombolysis. Moreover, the modified material maintained its functional efficacy after one month of PBS immersion, demonstrating excellent stability. Overall, this single-molecule multifunctional strategy may become a promising surface engineering technique for blood-contacting materials.

1. Introduction

Blood-contacting medical devices, such as central venous catheters, extracorporeal circulation circuits, and cardiovascular stents, play a crucial role in treating a variety of diseases [1–3]. However, when these devices made from foreign materials come into contact with blood, they almost inevitably trigger the activation of the coagulation system, leading to early device failure and increased risk of patient complications [4–6]. Despite decades of efforts by researchers to improve the hemocompatibility of these materials, thrombosis and related complications remain major challenges for blood-contacting medical devices [7–10].

In traditional clinical practice, patients using these devices may require long-term or even lifelong anticoagulation therapy [11–14]. However, these medications can lead to a range of side effects, such as thrombocytopenia and bleeding [15,16]. Consequently, in recent years, there has been increasing focus on research aimed at endowing implantable materials or devices with antithrombotic properties [17–21]. Various strategies have been employed to prevent thrombosis, including surface passivation [22–24] and the immobilization of anti-fouling molecules [25–30]. Regrettably, the efficacy of passive anti-fouling surfaces tends to diminish gradually over time, particularly in intricate pathological environments. In circulations, endothelium plays a crucial role in preserving vascular equilibrium via NO secreting

Peer review under responsibility of KeAi Communications Co., Ltd.
* Corresponding author. School of Materials Science and Engineering, Key Lab of Advanced Technology of Materials of Education Ministry, Southwest Jiaotong University, Chengdu, 610031, China.
** Corresponding author.
*** Corresponding author.
E-mail addresses: zhiluyang1029@swjtu.edu.cn (Z. Yang), tianwenjie1976@hotmail.com (W. Tian), huangnan1956@163.com (N. Huang).

https://doi.org/10.1016/j.bioactmat.2024.09.011
Received 21 August 2024; Received in revised form 7 September 2024; Accepted 7 September 2024

and glycocalyx structure. Inspired by the active surface of vascular endothelium, a common method to achieve anticoagulation is by mimicking the endothelial surface through the immobilization of active molecules produced by endothelial cells or components of the endothelial surface [31–34]. Examples include nitric oxide (NO) generators [35,36] and hyaluronic acid [27]. Although these surfaces can prevent clotting to some extent, due to prolonged contact with foreign surfaces, thrombosis on device surfaces remains difficult to completely prevent with these strategies. Another approach is to accept the inevitability of clot formation and design surfaces that can dissolve newly formed small clots [37–39]. Based on this concept, a strategy has been proposed to activate the fibrinolytic system to break down newly formed surface clots. To achieve this, the surfaces of blood-contacting materials are typically designed to have the capability to adsorb plasminogen (Plg) and plasminogen activators, such as tissue plasminogen activator (t-PA) [40–43]. This is because t-PA can activate Plg into plasmin, which binds to and dissolves the clot, thereby preventing vascular occlusion [44,45]. Over the past decade, effective fibrinolytic surfaces have typically been achieved by stably immobilizing high-density lysine (Lys) reagents [46,47]. Given the specific and strong affinity of Lys for Plg and t-PA, these Lys-rich surfaces dissolve clots by specifically binding Plg and its activators, generating plasmin upon contact with plasma. Thus, the integration of antithrombotic and fibrinolytic strategies may represent an optimal approach for addressing clotting on implant surface. The exploration of combining antithrombotic and fibrinolytic strategies for surface modification of implants with monocomponent bioactivity is limited. This limitation can be attributed to the challenges associated with traditional surface modification methods for incorporating multiple components, such as their lack of control, ease of use, and reproducibility. Herein, we report a novel single-molecule multifunctional strategy for creating biomimetic blood-compatible surfaces with endothelial-like and fibrinolytic properties. Specifically, we integrated Cu-DOTA-$(Lys)_3$, which features copper ions capable of catalyzing NO release and three Lys ligands, onto material surfaces. NO is an endogenous gaseous signaling molecule released by endothelial cells that can inhibit platelet activation and aggregation through a cyclic guanosine monophosphate (cGMP)-dependent pathway. Lys is a ligand with high affinity for Plg and t-PA, promoting plasmin generation to dissolve nascent clots. To combine these two ligands, Lys was covalently attached to azidated Cu-DOTA molecules, which have a strong capacity for coordinating copper ions and catalyzing NO release. The resulting complex was then grafted onto pre-DBCO-functionalized surfaces via click chemistry. A series of characterization methods and assays confirmed the successful preparation of these surfaces. Platelet adhesion and plasma clot dissolution experiments indicated that the dual-modified surfaces retained both affinity of Lys for Plg and t-PA and NO release functionalities, with these functions operating independently and without mutual interference.

2. Experimental and materials

2.1. Materials

N,N′-Dicyclohexylcarbodiimide (DCC, ≥99 %), 14-azidomethyl-3,6,9,12-tetraoxatetradecan-1-amine (N_3-PEG_4-NH_2, ≥90 %), tri-tert-butyl-1,4,7,10-tetraazacyclododecane-1,4,7,10-tetraacetate (DOTA-tris(tbu)ester, ≥95 %), 1-Hydroxy-2,5-pyrrolidinedione (HOSu, ≥99 %) Nα-(tert-butoxycarbonyl)-L-lysine (NH_2-LYS(BOC)-OH, ≥99 %), trifluoroacetic acid (TFA, ≥99 %), dimethyl sulfoxide (DMSO, ≥99.7 %), N-hydroxysuccinimide (NHS, ≥98 %), 1-(3-dimethylaminopropyl)-3-ethylcarbodiimide hydrochloride (EDC, ≥99.7 %), 1,2-ethanedithiol (EDT, ≥98 %), cupric chloride dihydrate ($CuCl_2{\cdot}2H_2O$, ≥99.7 %), dichloromethane (DCM, ≥99.5 %), dopamine (DA, ≥98 %), polyacrylamide (PAa, Mw~17000), Tris base (≥99 %), sodium ascorbate (≥99 %), copper (II) sulfate pentahydrate ($CuSO_4{\cdot}5H_2O$, ≥98 %), N,N′-diisopropylethylamine (DIPEA, ≥99.5 %), horseradish peroxidase substrate (HRP), L-glutathione (GSH, ≥98 %), S-Nitroso-N-acetyl-DL-penicillamine (SNAP, ≥97 %), bovine serum albumin (BSA, ≥98 %), 20X wash buffer, tissue-type plasminogen activator (t-PA, ≥95 %) were purchased from Sigma-Aldrich, China. Triethylamine (TEA, ≥99 %) was obtained from JT Baker Chemical Products Trading (Shanghai) Co., Ltd. Triisopropylsilane (TIS, 98 %) was obtained from Shanghai Darui Finechem Co., Ltd. Anhydrous ethanol, physiological saline, and glutaraldehyde solution were provided by Chengdu Kelong Chemical Co., Ltd. Activated Partial Thromboplastin Time (APTT) Kit was purchased from Shanghai Sunbio Medical Technology Co., Ltd. Dibenzocyclooctyne-PEG_4-N-hydroxysuccinimidyl (DBCO-PEG_4-NHS, ≥90 %) was provided by Xi'an Qiyue Biology Co., Ltd.

2.2. Synthesis of Cu-DOTA-$(Lys)_3$

The carboxyl groups in DOTA-tris(tbu)ester were first activated using DCC and HOSu. An equimolar amount of N_3-PEG_4-NH_2 and a triple molar amount of TEA were then added to the solution. The reaction was allowed to proceed for 2 h. Subsequently, a cleavage reagent consisting of 95 % TFA, 2 % EDT, 2 % TIS, and 1 % water was introduced and the mixture was stirred for an additional 2 h. The resulting solution was extracted with ether and lyophilized to obtain N_3-DOTA. Afterwards, N_3-DOTA was redissolved and reactivated using DCC and HOSu, followed by the addition of an equimolar amount of NH_2-LYS(BOC)-OH and a triple molar amount of TEA. The cleavage reagent was applied again to this mixture. Post-reaction, the solution was extracted with ether, resulting in the formation of N_3-DOTA-$(Lys)_3$ solution. This solution was purified using High-performance liquid chromatography (HPLC) on an Agilent Technologies LC200 system (United States). For obtaining Cu-DOTA-$(Lys)_3$ and Cu-DOTA, N_3-DOTA-$(Lys)_3$ and N3-DOTA were dissolved and mixed with an equimolar amount of $CuSO_4{\cdot}5H_2O$ and reacted for 30 min. The resultant solutions were frozen and dried, and the obtained Cu-DOTA-$(Lys)_3$ and Cu-DOTA were stored in vacuum for further use.

2.3. Characterization of N_3-DOTA-$(Lys)_3$

The molecular mass of N_3-DOTA-$(Lys)_3$ was confirmed by electrospray ionization mass spectrometry (ESI-MS) using a Waters ZQ 2000 system. The chemical structure of the molecule was analyzed by proton nuclear magnetic resonance (^{1}H NMR) spectroscopy on a Bruker Ultrashield 600 MHz NMR spectrometer. The ultraviolet–visible (UV–Vis) spectroscopy analysis was performed using a 752N spectrophotometer (Beijing General Analysis Technology Co., Ltd.).

2.4. Preparation of amine-rich Am-pDA coating

316L stainless steel (SS, 1 × 1 cm) were immersed in a Tris-HCl buffer solution containing 1 mg/mL DA. This reaction was carried out at 25 °C for 12 h to form polydopamine (pDA) coating on the substrate. Then, the pDA-coated 316L SS samples were immersed in a PAa solution (3.5 mg/mL) with a pH value of 10. The reaction was allowed to proceed for 12 h at 25 °C for increasing the surface density of amine groups. Afterwards, the coated samples were cleaned and dried for further use and named as Am-pDA.

2.5. Preparation of Cu-DOTA and Cu-DOTA-$(Lys)_3$ coating

NHS-$(PEG)_4$-DBCO (2 mg/mL) was dissolved in a solvent mixture of PBS and DMSO with 1:1 vol ratio. Then, the Am-pDA coated samples were dipped into the NHS-$(PEG)_4$-DBCO solution and incubated at 25 °C in dark environment for 12 h, transferring the surface amine groups to DBCO groups. Subsequently, the samples were immersed in a PBS solution containing 2 mg/mL of Cu-DOTA or Cu-DOTA-$(Lys)_3$ with pH value of 8 adjusted by DCC, achieving the grafting of Cu-DOTA or Cu-DOTA-$(Lys)_3$.

2.6. Characterization of Cu-DOTA-(Lys)$_3$ coating

The chemical structure of Cu-DOTA-(Lys)$_3$ coating was analyzed by Fourier-transform infrared (FTIR) spectra using a Nicolet 5700 (Thermo Fisher Scientific, USA). The reflectance scanning mode was employed with a wavelength measurement range of 500–4000 cm^{-1}. The chemical composition and elemental content were examined using an AXIS-ULTRA DLD X-ray photoelectron spectrometer (XPS) from Beijing Instrument Link Four Seas Technology Co., Ltd. The real-time monitoring of Cu-DOTA-(Lys)$_3$ grafting was conducted using a quartz crystal microbalance instrument (QCM-D, Q-sense AB, Sweden). The Am-pDA coating was first prepared on a 5 MHz quartz crystal surface and placed into the chamber. A steady baseline was achieved by flowing PBS buffer at a rate of 50 μL/min for 40 min. The buffer was then replaced with a pre-prepared Cu-DOTA-(Lys)$_3$ solution and maintained for about 20 h until the curve stabilized. Physical adsorption of the molecules was removed by pumping fresh PBS buffer after grafting. The density of amine groups, including primary, secondary and tertiary amines, on the modified SS samples was quantified using a colorimetric staining method. In detail, modified SS were incubated in Acid Orange II (AO, 500 nM, pH 3) for 12 h at 37 °C, followed by rinsing with HCl solution (pH 3) three times. Then, samples were incubated in NaOH solution (pH 12) for 15 min at 37 °C to dissolve the combined AO on the surface. The AO concentration in the NaOH solution was using an enzyme marker (μQuant, Bio-tek Instruments Inc.) at 485 nm. The density of amine groups was calculated using the standard curve of AO.

2.7. NO catalytic release of Cu-DOTA-(Lys)$_3$ coating

The real-time NO catalytic release rate of Cu-DOTA-(Lys)$_3$ coating was determined using a nitric oxide analyzer (NOA Seivers 280i). Before detection, all the samples were pre-immersed in plasma for Plg adsorption. The detection temperature was set at 37 °C to simulate the human body temperature. Then, PBS solution containing 10 μM GSH and 10 μM SNAP was placed in the reaction vessel for 10 min to record the baseline. Then, Cu-DOTA-(Lys)$_3$ coated SS was immersed into the solution and the NO release was recorded. To assess the durability of NO catalytic release capability of the Cu-DOTA-(Lys)$_3$ coating, the modified SS samples were immersed in PBS for 30 days at 37 °C. After immersion, the NO catalytic release of the coating was detected.

2.8. In vitro platelet adhesion and activation on Cu-DOTA-(Lys)$_3$ coating

Rabbit platelet rich plasma was obtained by centrifugation at a centrifugal force of 25 g for 15 min. Before PRP incubation, all the samples (316L SS, 1 cm × 1 cm) were pre-immersed in plasma for Plg adsorption. The sample was then rinsed with a sodium chloride solution three times, for 30 s each time, followed by treatment with t-PA (0.1 mg/mL) to address the actual adsorption of Plg. After activation, the samples were incubated with 200 μL of PRP and 10 μL NO donor solution (10 μM GSH and 10 μM SNAP in saline) for 30 min at 37 °C. Subsequently, the samples were rinsed with saline solution and fixed in 2.5 % glutaraldehyde solution, followed by the dehydration, dealcoholizing and critical point drying. Afterwards, scanning electron microscopy (SEM) was performed to observe the adhered platelets on the samples. cGMP expression of platelets after incubation was measured by a cGMP ELISA kit.

2.9. Plasminogen adsorption on Cu-DOTA-(Lys)$_3$ coating

To confirm the Plg adsorption behavior on the Cu-DOTA-(Lys)$_3$ coating, the coated samples were first immersed in 200 μL of plasma at 37 °C for 3 h. Then, the samples with adsorbed Plg were blocked by BSA (1 %) and incubated at 37 °C for 90 min, followed by the incubation with Horseradish Peroxidase-Streptavidin conjugate at 37 °C for 60 min. Subsequently, the TMB was added and incubated for 30 min, and the absorbance at 450 nm was measured. Note that the samples were rinsed with PBS three times, for 1 min each time, after each immersion.

2.10. Thrombolytic performance of Cu-DOTA-(Lys)$_3$ coating

All the samples were first incubated in 200 μL of plasma at 37 °C for 3 h. After carefully cleaning, the samples were treated with t-PA (0.1 mg/mL) for the activation of adsorbed Plg. Subsequently, 100 μL of plasma supplemented with 100 μL of $CaCl_2$ solution (0.025 mol/L) was dropped on the surfaces of samples. The absorbance of the plasma at 405 nm was continuously recorded for a duration of 80 min. To evaluate the durability of Cu-DOTA-(Lys)$_3$ coating in thrombolytic performance, the coated samples were immersed in PBS for 30 days at 37 °C. After that, the thrombolytic performance of samples was assessed as mentioned above.

Ethics approval

The animal experiments were approved by the Animal Ethics Committee of Dongguan Hospital Affiliated to Southern Medical University. The ethical approval Number was IACUC-AWEC-202311111.

2.11. Ex vivo anti-thrombogenicity of Cu-DOTA-(Lys)$_3$ coating

A New Zealand white rabbit arteriovenous (AV) shunt model was performed for *ex vivo* thrombogenicity test. Briefly, the bare and modified SS foil were first incubated in 200 μL of plasma at 37 °C for 3 h. After carefully cleaning, the samples were treated with t-PA (0.1 mg/mL) for the activation of adsorbed Plg. After that, the SS foils were placed into the PVC catheters, which were connected to the left carotid artery and the right jugular vein of rabbits to form a closed loop. The rabbits did not receive anticoagulants before or during the surgery. A 2 mL solution of 10 μM donor was injected prior to circulation. After 2 h of *ex vivo* blood circulation, the PVC catheters were removed and rinsed with saline solution. The side-view of the catheters and the surface morphology of samples were photographed. Meanwhile, the occlusion ratio was determined by calculating the ratio of the thrombus area to the internal area of catheters according to the cross-section images. The thrombus formed on the foil surface was weighed and observed by SEM.

2.12. Blood analysis by ex vivo blood circulation

The blood samples were collected from New Zealand white rabbits during *ex vivo* blood circulation test at various intervals (0, 5, 30 and 60 min) for comprehensive hematological and biochemical assessments. To mimic real-world practice, a prolonged catheter (length 1.6 m, inner diameter 3 mm) was chosen to obtain more contact area of lumen surface to the blood. Subsequent to the collection, blood analysis was carried out, including assessments of white blood cell count (WBC), platelet count (PLT), Alanine Aminotransferase (ALT) levels, serum creatinine (Scr), activated partial thromboplastin time (APTT), and levels of prothrombin fragment 1 + 2 (F1+2). Additionally, the concentrations of complement component 3a (C3a), C-reactive protein (CRP), interleukin 10 (IL-10), and tumor necrosis factor alpha (TNF-α) were also measured.

2.13. Statistical analysis

All data were presented as mean ± standard deviation (SD) from at least four independent experiments. Statistical significance was determined using one-way ANOVA. Significance levels are indicated in the figures as follows: *$p < 0.05$, **$p < 0.01$, and ***$p < 0.001$.

3. Results and discussion

3.1. Synthesis of Cu-DOTA-(Lys)$_3$

In this study, we utilized the classical Boc solid-phase synthesis method to conjugate two key active molecules: DOTA-tris(tbu)ester and Boc-protected Lys to azide-bearing PEG fragments, resulting in the successful synthesis of azide-terminated bio-functional molecules (Fig. 1A). To achieve high-purity bio-functional molecules, we purified N_3-DOTA-(Lys)$_3$ using high-performance liquid chromatography (HPLC), obtaining a purity of 96.6 % (Fig. 1B). Following purification, we characterized the molecular structure of synthesized molecules using nuclear magnetic resonance (NMR) spectroscopy and electrospray ionization mass spectrometry (ESI-MS). The results demonstrated that the mono-isotopic mass of the azide compound [M+H]+was 1034.19, consistent with its theoretical molecular weight of 1033.24 (Fig. 1C). Additionally, ^{1}H NMR analysis exhibited all characteristic peaks of DOTA, Lys, and N_3-PEG$_4$-NH$_2$ in N_3-DOTA-(Lys)$_3$, further confirming its successful construction (Fig. 1D). Then, we confirmed the feasibility of Cu chelation of synthesized N_3-DOTA-(Lys)$_3$ by UV–Vis with a signal appearing at 270 nm, which indicated successful chelation of Cu^{2+} to DOTA-(Lys)$_3$, (Fig. 1E and F). These findings confirmed the successful synthesis of Cu-DOTA-Lys with endothelial and fibrinolytic properties.

3.2. Preparation and characterization of Cu-DOTA-(Lys)$_3$ surfaces

The preparation of the Cu-DOTA-(Lys)$_3$ surface involved several steps, as illustrated in Fig. 2A. First, a Am-pDA coating rich in amino groups was constructed on the 316L SS surface following an established method [48,49]. To confirm the successful construction of the amine-rich coating, we performed FTIR analysis (Fig. S1). The increase in the double peaks of alkane at 2936 and 2858 cm^{-1} and the peak of -N-H at 1588 cm^{-1} indicated the introduction of PAa. Moreover, the peaks at 1635 cm^{-1} and 1288 cm^{-1}, corresponding to the stretching vibrations of aromatic C=N and aromatic C-O, respectively, showed enhancement and reduction. This indicated that the binding of PAa to pDA is most likely facilitated through a Schiff base reaction. This hypothesis was further corroborated by high-resolution spectra obtained from XPS (Fig. S2). Specifically, the Am-pDA coating exhibited a higher proportion of C-N and aliphatic N-H components, along with a decrease in C=O content and an increase in CN content relative to pDA, suggesting the schiff-base reaction between -NH$_2$ in PAa and C=O in pDA. The results of amino quantification indicated that after introducing PAa, the amine group increased by 81.4 % (Fig. S3). This significant increase demonstrated the potential of this coating as a promising amine-rich platform for subsequent grafting applications.

In order to enable the material surface to catalyze NO release and specifically capture Plg and tPA, we grafted NHS-(PEG)$_4$-DBCO onto the Am-pDA surface using carbodiimide chemistry. Subsequently, through a

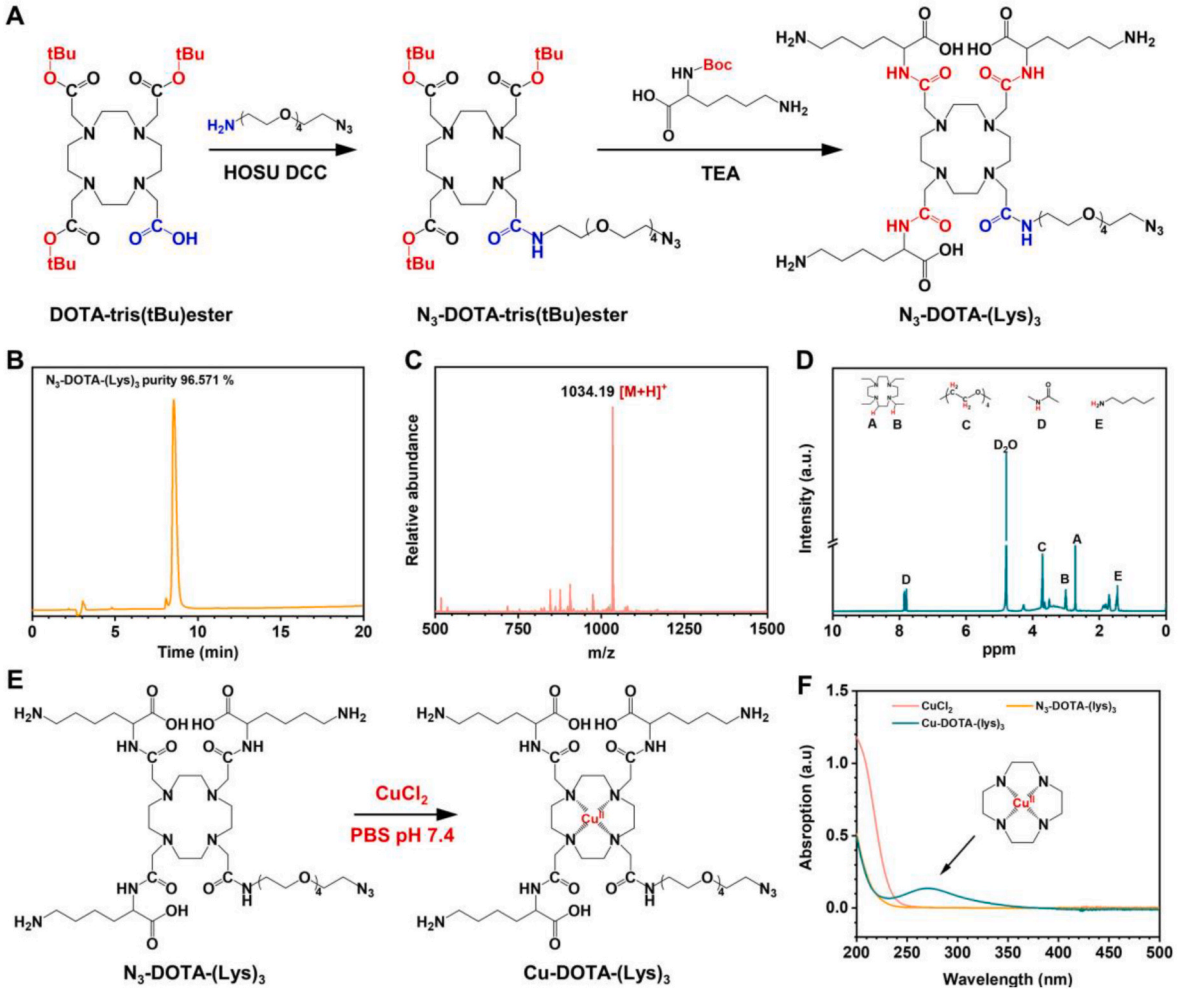

Fig. 1. Synthetize and characterization of N_3-DOTA-(Lys)$_3$ and Cu-DOTA-(Lys)$_3$. (A) Synthetic route of N_3-DOTA-(Lys)$_3$. High-performance liquid chromatography spectrum. (B) Electrospray ionization mass spectrum (C) and ^{1}H NMR spectrum of N_3-DOTA-(Lys)$_3$. (E) Synthetic route of Cu-DOTA-(Lys)$_3$. (F) UV–vis spectra of Cu-DOTA-(Lys)$_3$.

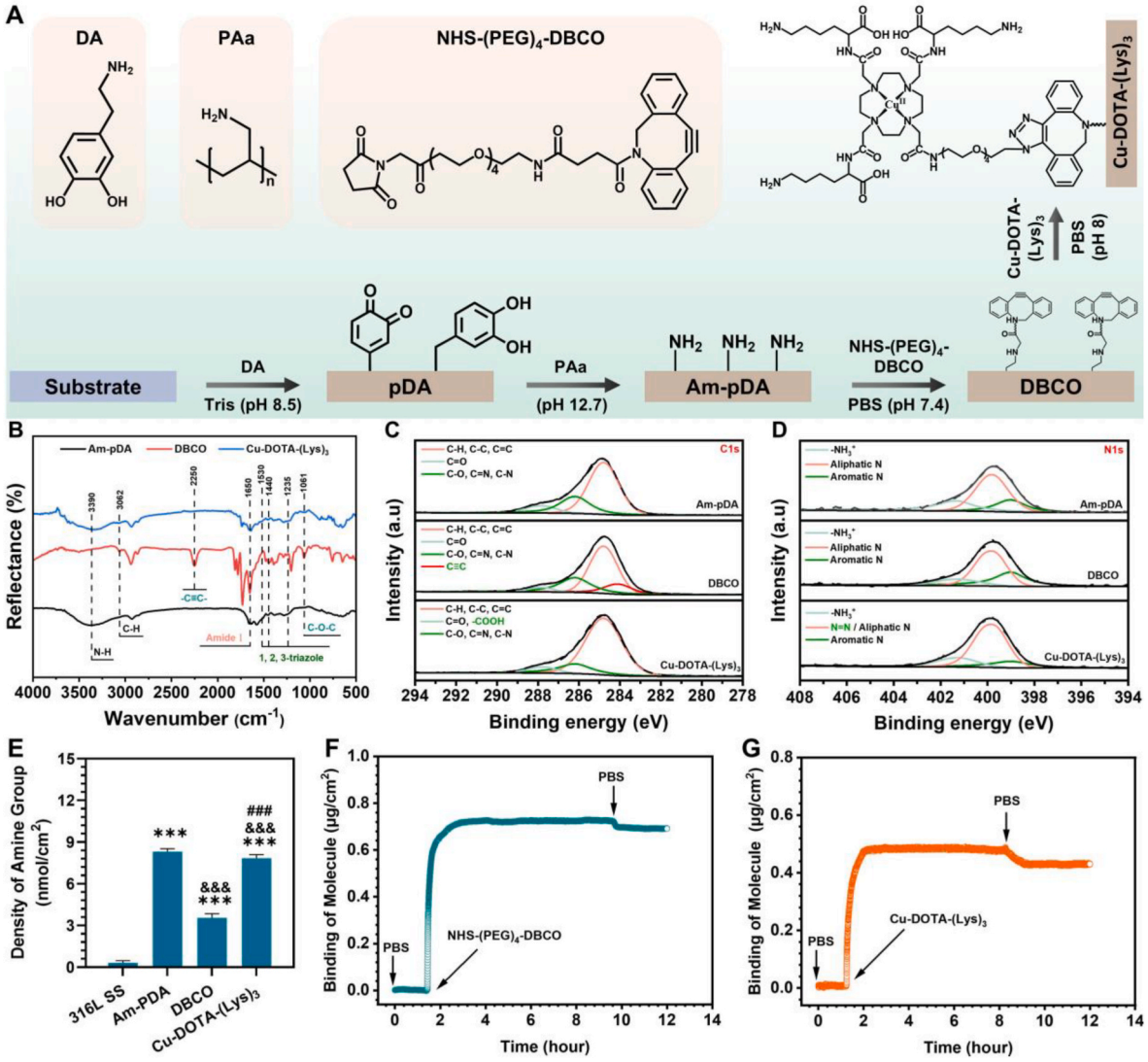

Fig. 2. Fabrication and characterization of different surface. (A) Schematic depicting the procedure for preparation of Cu-DOTA-$(Lys)_3$ surfaces. (B) FTIR and high-resolution XPS spectra of (C) C 1s and (D) N 1s for Am-pDA, DBCO and Cu-DOTA-$(Lys)_3$. (E) Quantitative analysis of surface amine group density for Am-pDA, DBCO and Cu-DOTA-$(Lys)_3$. QCM-D real-time monitoring of the grafting amount of (F) NHS-$(PEG)_4$-DBCO and (G) Cu-DOTA-$(Lys)_3$ on Am-pDA or NHS-$(PEG)_4$-DBCO-modified Au chip. * Compared with 316L SS, & with Am-pDA, and # with DBCO; one symbol indicates $p < 0.05$, two symbols indicate $p < 0.01$, and three symbols indicate $p < 0.005$. ($n = 4$, mean ± SD).

DBCO-N_3 bio-orthogonal reaction [50,51], Cu-DOTA-$(Lys)_3$ was grafted to the DBCO-functionalized surface. To confirm the successful covalent grafting of Cu-DOTA-$(Lys)_3$, FTIR and XPS analyses were performed. As shown in Fig. 2B, the characteristic peak of the DBCO ring (C ≡ C, 2250 cm^{-1}) disappeared in the FTIR spectrum, while a set of triazole peaks appeared, indicating an effective bio-orthogonal reaction between DBCO and the azide residues. XPS analysis further corroborated the successful grafting of Cu-DOTA-$(Lys)_3$ (Fig. S4 and Table S1). High-resolution spectra analysis of C1s revealed an increase in the peak at 284.1 eV after NHS-PEG-DBCO modification, which was assigned to the C ≡ C bond in DBCO, then this peak disappeared after Cu-DOTA-$(Lys)_3$ grafting, corresponding to the transformation from C ≡ C to triazole. Moreover, a visible decrease in -NH_3^+ and an increase in aromatic nitrogen were observed in the DBCO group compared to Am-pDA group, which may be induced by the consumption of -NH_3^+ in Am-pDA and the introduction of DBCO. After Cu-DOTA-$(Lys)_3$ modification, the significant increase in -NH_3^+ and N=N indicated the formation of triazole and the introduction of Cu-DOTA-$(Lys)_3$ (Fig. 2C and D).

The grafting amount of Cu-DOTA-$(Lys)_3$ on the Am-pDA coating was quantified by measuring the density of surface amino groups and further verified by QCM-D measurement. As shown in Fig. 2E, the amino group density on the Am-pDA surface significantly decreased after NHS-$(PEG)_4$-DBCO grafting, indicating the successful grafting of NHS-$(PEG)_4$-DBCO. Interestingly, when Cu-DOTA-$(Lys)_3$ was grafted onto the samples, the amino group density significantly increased due to the amino groups on the Lys molecules, further confirming the successful grafting of Cu-DOTA-$(Lys)_3$ molecules. To further verify the amount of Cu-DOTA-$(Lys)_3$ grafted onto the material surface, QCM-D measurements were performed. The results showed that the grafting densities of NHS-$(PEG)_4$-DBCO and Cu-DOTA-$(Lys)_3$ were 622 ng/cm^2 and 415 ng/cm^2, respectively (Fig. 2F and G). According to our study, this density surpasses that of most current surface modification platforms [37]. Moreover, the high-density grafting contributes to enhanced fibrinolytic capacity [46].

3.3. *In vitro* NO catalytic release and blood compatibility tests

In this study, GSH in the NO donor solution reduces Cu^{2+} chelated by DOTA to Cu^{+}. This process further catalyzes the formation of NO from SNAP [52]. Subsequently, the generated NO inhibits platelet adhesion

and activation by upregulating cGMP levels within the platelets, thereby achieving the anticoagulant function of the coating (Fig. 3A) [53,54]. The catalytic NO release activity on the Cu-DOTA-$(Lys)_3$ surface was evaluated using real-time chemiluminescence. As shown in Fig. 3B and C, the amounts of NO released from the surfaces of Cu-DOTA and Cu-DOTA-$(Lys)_3$ were measured to be 6.08 ± 0.34 and 5.91 ± 0.81 × 10^{-10} mol cm^{-2} min^{-1}, respectively. This indicates that even when Lys on the Cu-DOTA-$(Lys)_3$ surface binds Plg, the ability of the copper ion to catalyze NO release remains unaffected. Thrombosis has always been a primary issue for blood-contacting materials, and NO can inhibit platelet aggregation into a clot. To assess the ability of NO released by Cu-DOTA and Cu-DOTA-$(Lys)_3$ surfaces to promote cGMP synthesis in platelets, cGMP analysis was conducted (Fig. 3D). The results showed that Cu-DOTA and Cu-DOTA-$(Lys)_3$ surfaces significantly upregulated cGMP expression. Moreover, there was no significant difference in cGMP expression between the two NO-releasing surfaces, consistent with the NO release results.

Subsequently, we further investigated platelet adhesion and activation states on different surfaces. After adding the donor to all sample groups, a substantial number of platelets adhered to the 316L SS and DBCO groups, exhibiting significant activation and aggregation. Additionally, the DOTA-$(Lys)_3$ group, which only possesses fibrinolytic capability, still showed noticeable platelet adhesion and activation. In contrast, Cu-DOTA group significantly reduced platelet adhesion and activation, keeping them in an inactive spherical state. (Fig. 3E and G). These results suggested that NO gas molecules effectively inhibit thrombosis in the blood microenvironment.

It is worth noting that after treating the Cu-DOTA-$(Lys)_3$ coating in PBS for 30 days (Fig. S5), its catalytic release of NO retained 65.8 % of its original level, which remains within the effective range for exerting anticoagulant activity [33]. In summary, these results demonstrated that Cu-DOTA-$(Lys)_3$ surfaces exhibit excellent *in vitro* antithrombotic properties.

3.4. Plasma clot lysis

When fibrin clots form within the body, Plg and t-PA bind to the C-terminal Lys residues on the clot surface through Lys binding sites, creating a ternary complex. t-PA converts Plg into plasmin, which degrades the fibrin network into soluble fibrin degradation products (Fig. 4A). Thus, Plg plays a crucial role throughout the thrombolytic process [55]. In this study, we measured the adsorption of Plg on various samples in plasma. As shown in Fig. 4B, surfaces without Lys exhibited lower Plg adsorption (~21 ng/cm^2). In contrast, the introduction of Lys increased Plg adsorption on DOTA-$(Lys)_3$ and Cu-DOTA-$(Lys)_3$ surfaces by 13-fold (~275 ng/cm^2). Notably, there was no difference in Plg adsorption between DOTA-$(Lys)_3$ and Cu-DOTA-$(Lys)_3$ surfaces (p = 0.9269), indicating that copper ion-catalyzed NO release does not affect

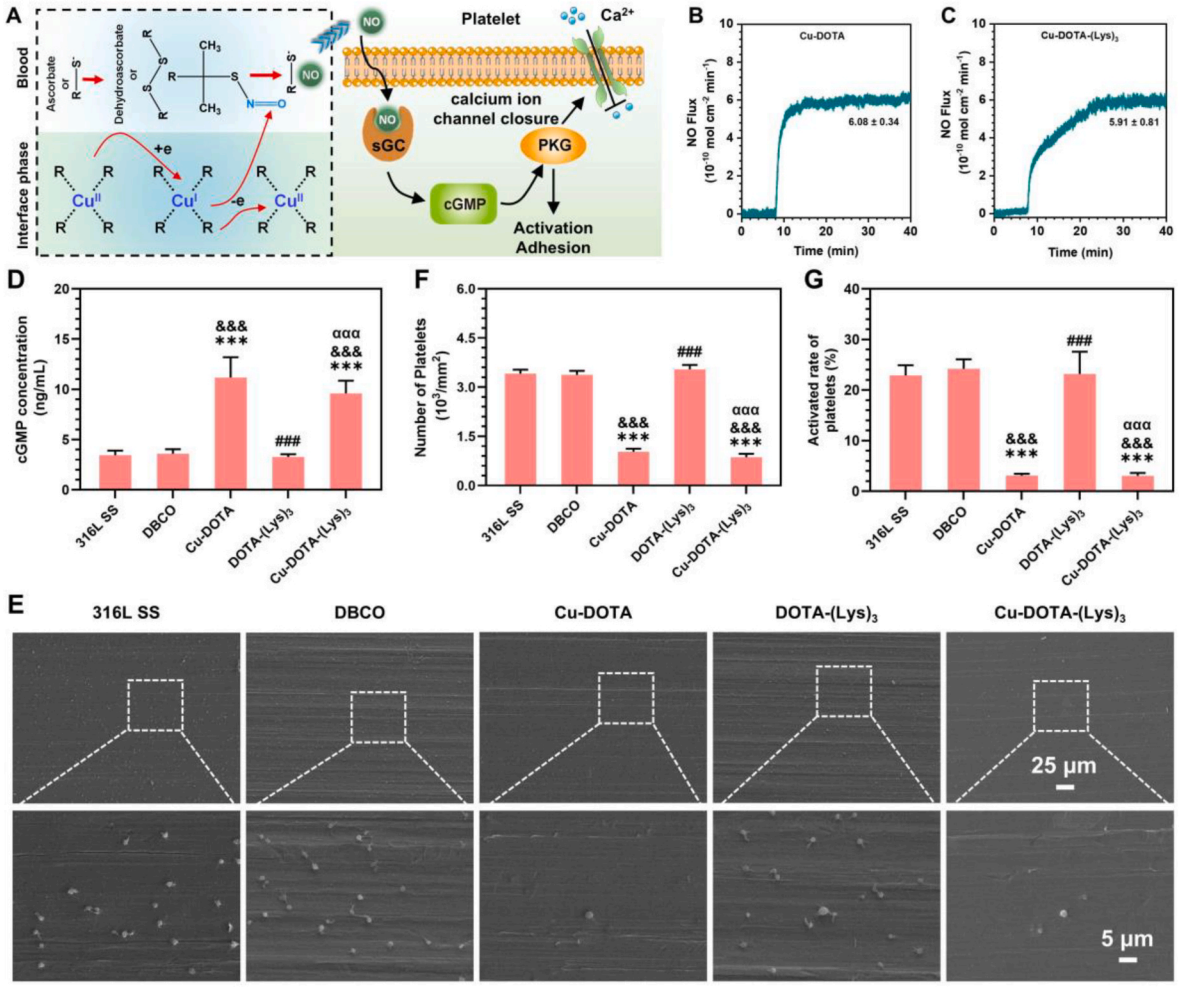

Fig. 3. *In vitro* NO catalytic release and blood compatibility tests. (A) Schematic diagram of NO release catalyzed by copper ions. (B) Real-time release of NO induced by (B) Cu-DOTA and (C) Cu-DOTA-$(Lys)_3$. (D) cGMP concentration of the adherent platelet on different samples. (E) SEM image of the adherent platelets (F) amount of the adherent platelets and (G) activation rate of adherent platelets on bare or modified 316L SS. * Compared with 316L SS, & with DBCO, # with Cu-DOTA and α with DOTA-$(Lys)_3$; one symbol indicates $p < 0.05$, two symbols indicate $p < 0.01$, and three symbols indicate $p < 0.005$. (n = 4, mean ± SD).

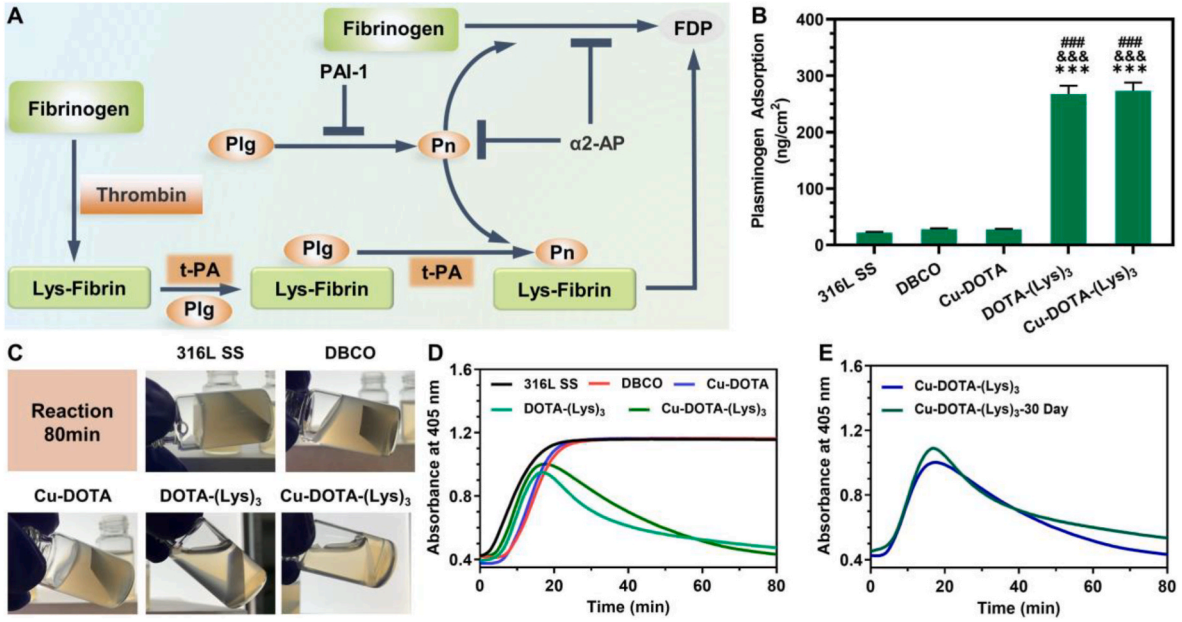

Fig. 4. The fibrinolysis of coatings. (A) Schematic representation of the major reactions of fibrinolysis. The black arrows indicate biochemical transformations involving protein hydrolysis and cleavage. The T-shaped symbol represents an inhibitory effect. The C-terminal Lys residues on fibrin (Lys-Fibrin), plasminogen (Plg), and plasmin (Pn) are released and bind to fibrin in the presence of fibrin clots, leading to their activation. t-PA converts circulating Plg into plasmin, which digests fibrin clots to form fibrin degradation products (FDP). Excessive enzymes are inactivated to restore hemostatic balance by plasminogen activator inhibitor-1 (PAI-1) and α2-antiplasmin (α2-AP). (B) Adsorption of Plg from plasma on different samples. (C) The visual appearance of the plasma at 80 min of reaction for different samples. Clot formation in plasma expressed as absorbance at 405 nm versus for different samples (D) and Cu-DOTA-$(Lys)_3$ (E) (immersion for 1 or 30 days in PBS). * Compared with 316L SS, & with DBCO, # with Cu-DOTA and α with DOTA-$(Lys)_3$; one symbol indicates $p < 0.05$, two symbols indicate $p < 0.01$, and three symbols indicate $p < 0.005$. ($n = 4$, mean ± SD).

the binding of Plg to Lys. The study suggests that a Lys-modified surface with Plg adsorption levels reaching 40 ng/cm^2 exhibits fibrinolytic activity [56]. Therefore, DOTA-$(Lys)_3$ and Cu-DOTA-$(Lys)_3$ surfaces are expected to have similar fibrin-dissolving capabilities.

To verify this hypothesis, we immersed all samples in plasma to adsorb a layer of Plg via Lys residues. Plg adsorbed in this manner was converted into plasmin through t-PA treatment. The samples were then immersed in recalcified citrated plasma. As shown in Fig. 4C, after 80 min of reaction, Lys-containing surfaces effectively dissolved clots. Further, we assessed the clot-dissolving properties of modified surfaces using an optical plasma coagulation assay by measuring the absorbance of plasma at 405 nm over time. As shown in Fig. 4D, the absorbance curve sharply increased over time upon initial clot formation. For 316L SS, DBCO, and Cu-DOTA surfaces without Lys, absorbance reached a plateau after 20 min. Conversely, for Lys-containing surfaces, absorbance increased during the first 20 min and then declined, returning to baseline after 60 min. These observations indicate that despite initial clot formation, the nascent clot was rapidly cleaved by surface-localized plasmin. Interestingly, Cu-DOTA-$(Lys)_3$ surfaces exhibited almost the same fibrinolytic activity as DOTA-$(Lys)_3$ surfaces, suggesting that NO release do not affect Lys activity. Notably, Cu-DOTA-$(Lys)_3$ surfaces also demonstrated good fibrinolytic stability, retaining their fibrinolytic capacity after 30 days of continuous treatment with NO donor-containing solutions (Fig. 4E). This implies that such surfaces were suitable for long-term blood-contacting devices.

3.5. Ex vivo anti-thrombogenicity

Encouraged by the results of *in vitro* anticoagulation and fibrinolysis experiments, we hypothesized that the coating could exhibit good anticoagulant properties in a blood environment [57]. As shown in Fig. 5A, when the material comes into contact with blood, copper ions catalyze the release of NO from endogenous S-nitrosoglutathione (RSNO), thereby inhibiting platelet adhesion and activation, achieving anticoagulation. When a fibrin network forms, Lys specifically captures t-PA and Plg to dissolve the fibrin, achieving thrombolysis. To verify its effectiveness in a blood environment, we prepared coating materials rich in Plg and used a New Zealand rabbit arteriovenous shunt model to evaluate the anticoagulant performance of the coating through *ex vivo* blood circulation tests (Fig. 5B). After 2 h of circulation, the bare 316L stainless steel, Am-pDA, and DBCO-functionalized 316L stainless steel were almost completely occluded. In contrast, the Cu-DOTA-$(Lys)_3$ coating had almost no thrombi (Fig. 5C and D). Scanning electron microscopy (SEM) analysis (Fig. 5E) showed typical thrombus formation on the bare 316L stainless steel and DBCO foils, characterized by platelets and red blood cells embedded within a fibrin network. Notably, on the Cu-DOTA-$(Lys)_3$ modified 316L stainless steel, there were almost no thrombus such as platelets and red blood cells. Further quantitative analysis confirmed that the Cu-DOTA-$(Lys)_3$ modified 316L stainless steel exhibited excellent antithrombotic performance. Compared to bare 316L stainless steel, the thrombus weight (24.8 mg vs. 4.1 mg) and occlusion rate (92.3 % vs. 10.7 %) were significantly reduced. Correspondingly, the blood flow rate in the shunt also showed similar results. These findings are consistent with the *in vitro* anticoagulation results. Overall, the data indicate that the Cu-DOTA-$(Lys)_3$ group possesses superior *in vivo* antithrombotic performance.

3.6. Blood biochemical analysis

For blood-contacting devices, particularly those requiring large contact area or medium to long-term retention, such as central venous catheters and intravascular filters, it is crucial to thoroughly evaluate the impact of coating modifications on blood components as well as liver and kidney functions to ensure their safety for *in vivo* use [58]. In this study, we conducted *ex vivo* animal experiments using bare and Cu-DOTA-$(Lys)_3$ coated PVC catheters with an inner diameter of 3 mm and a length of 1.6 m to assess the effects of the coating on various biochemical and physiological blood parameters, including coagulation,

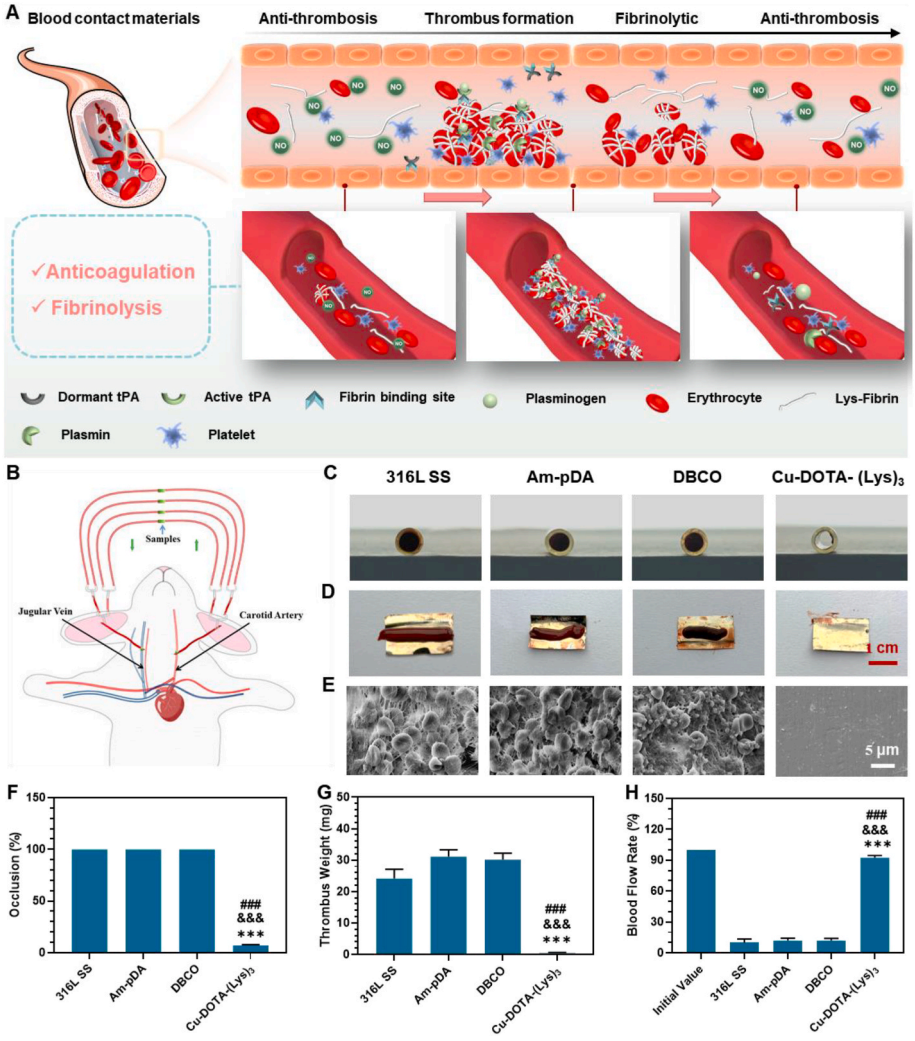

Fig. 5. *Ex vivo* hemocompatibility evaluation for bare or coated 316L SS. (A) Schematic diagram of the mechanism of action of Cu-DOTA-$(Lys)_3$ in contact with blood. (B) Schematic diagram of a rabbit arteriovenous shunt model for sample connection. Optical photos of cross-sectional thrombi (C) and thrombi on the surface of unfolded stainless-steel sheets (D) of different samples. (E) Characterize the surface morphology of different samples through SEM. (F) Occlusion, (G) thrombus weight, and (H) blood flow rate of different samples following the blood circulation. * Compared with 316L SS, & with DBCO, # with Cu-DOTA and α with DOTA-$(Lys)_3$; one symbol indicates $p < 0.05$, two symbols indicate $p < 0.01$, and three symbols indicate $p < 0.005$. ($n = 4$, mean ± SD).

inflammatory response, and liver and kidney functions (Fig. 6A).

Coagulation results indicated that the control group exhibited a higher tendency for blood coagulation after prolonged blood contact, evidenced by elevated levels of F1+2, an overall marker of prothrombin activation. There were no significant changes in APTT and PLT in either group (Fig. 6B–D). Upon device implantation, the device may be rapidly recognized by the immune system, potentially leading to an inflammatory response. However, no significant changes were observed in pro-inflammatory parameters, including C3a (C3 cleavage fragment indicating activation of the classical or alternative complement pathways), C-reactive protein (a plasma acute-phase protein used to measure acute inflammation), leukocytes (cells involved in immune responses), TNF-α (a pro-inflammatory cytokine), and IL-10 (a recognized anti-inflammatory and immunosuppressive cytokine) (Fig. 6E–I). These results suggest that none of the groups significantly affected the body's inflammatory indicators. To determine if the coating posed any significant toxicity risk to organs and tissues, we measured the blood concentrations of ALT and Scr, which are related to liver and kidney functions. The results showed no evidence of organ and tissue toxicity during circulation for PVC and Cu-DOTA-$(Lys)_3$-grafted surfaces, demonstrating their biosafety (Fig. 6J and K).

The experimental results indicate that the Cu-DOTA-$(Lys)_3$ anticoagulant biomimetic endothelial coating exhibits good blood compatibility when in contact with blood, without causing significant immunogenic issues within a short period. Therefore, the Cu-DOTA-$(Lys)_3$ anticoagulant biomimetic endothelial coating has excellent safety performance, showing great potential for surface modification of blood-contacting devices.

4. Conclusion

In summary, we have developed an innovative single-molecule multi-functional strategy to create blood-compatible surfaces with long-term anticoagulant and clot-dissolving properties, thereby ensuring sustained blood compatibility. These specific functions are achieved by immobilizing a single molecule with dual functions on the surface via click chemistry. The resulting Cu-DOTA-$(Lys)_3$ surface resists platelet adhesion and activation in plasma while selectively adsorbing Plg to enhance fibrinolytic activity. Additionally, these two functions were not compromised by the presence of each other. This approach uniquely integrates nitric oxide (NO) release and fibrinolysis into a singular bioactive molecule, thereby avoid the competition inherent in traditional fixation of multiple functional molecules and enabling precise control over their quantities on the surface. Notably, the modified

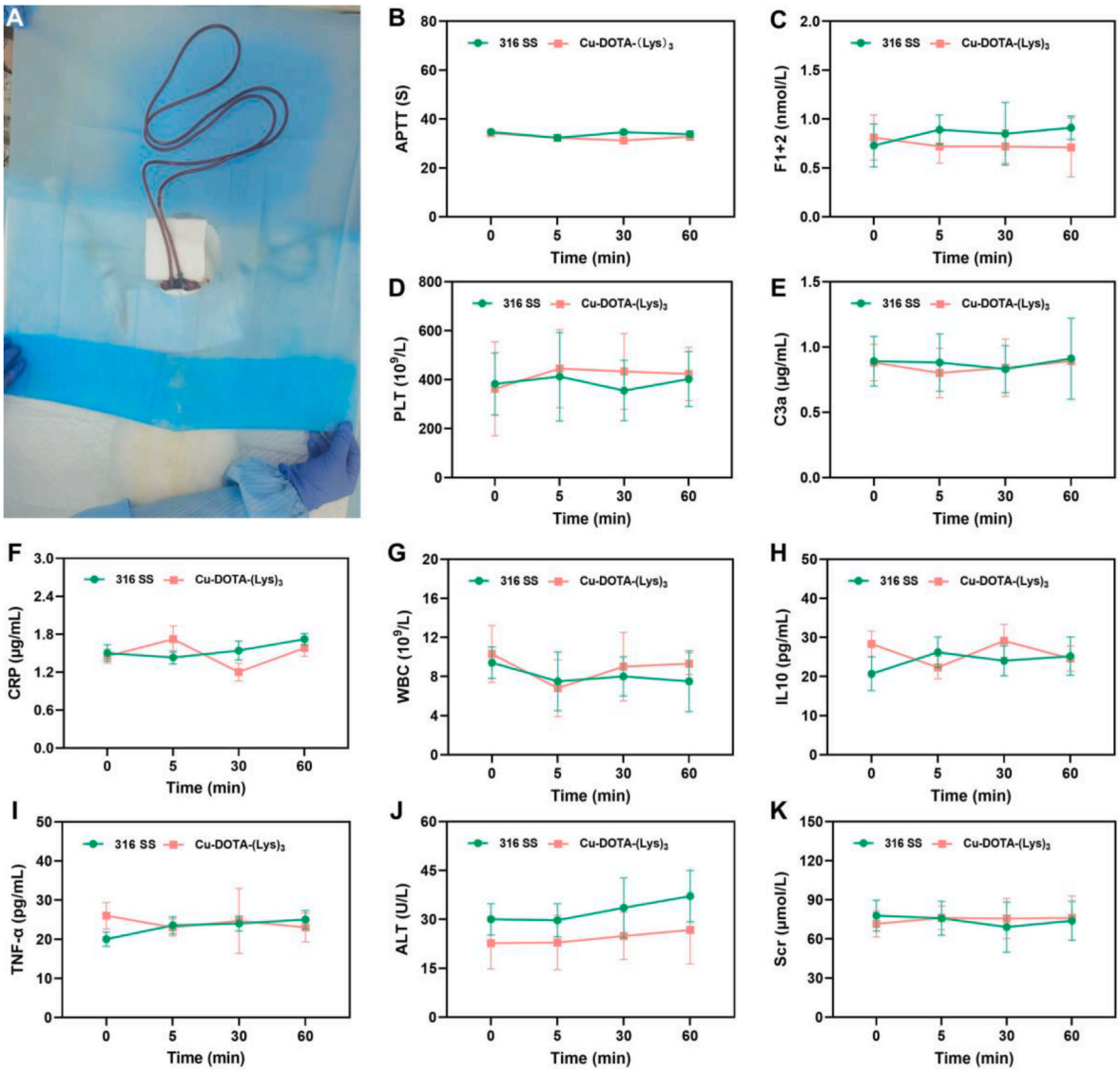

Fig. 6. Evaluation of coating blood routine and blood biochemistry. (A) Rabbit model for blood analysis. Coagulation related factors including (B) activated partial thromboplastin time (APTT), (C) F1+2 (an integral marker for prothrombin activation), and (D) platelet count (PLT). Inflammatory-associated factors including (E) C3a (a fragment produced by cleavage of C3), (F) C-reactive protein (CPR), (G) white blood cell count (WBC), (H) interleukin 10 (IL-10), and (I) Tumor necrosis factor-α (TNF-α). (J) Alanine aminotransferase (ALT) as a marker for liver function, and (K) serum creatinine (Scr) as a marker for kidney function. (n = 4, mean ± SD).

material demonstrated excellent stability, maintaining its functional efficacy for at least one month. Overall, this innovative single-molecule multifunctional strategy holds great potential as a surface engineering technique for blood-contacting materials, promising to advance the development of antithrombotic surfaces for biomedical applications.

Ethics approval and consent to participate

The animal experiments were approved by the Animal Ethics Committee of Dongguan Hospital Affiliated to Southern Medical University (Approval number IACUC-AWEC-202311111).

Data availability statement

Data will be made available on request.

CRediT authorship contribution statement

Wenxuan Wang: Writing – original draft, Visualization, Investigation. **Qing Ma:** Writing – original draft, Investigation. **Da Li:** Investigation, Data curation. **Wentai Zhang:** Writing – review & editing. **Zhilu Yang:** Writing – review & editing, Supervision, Funding acquisition, Conceptualization. **Wenjie Tian:** Writing – review & editing, Supervision, Conceptualization. **Nan Huang:** Writing – review & editing, Supervision, Funding acquisition, Conceptualization.

Declaration of competing interest

Zhilu Yang is an editorial board member for Bioactive Materials and was not involved in the editorial review or the decision to publish this article. Nan Huang is currently employed by GuangZhou Nanchuang Mount Everest Company for Medical Science and Technology. All authors declare that there are no competing interests.

Acknowledgements

This work was supported by the National Natural Science Foundation of China (Project 32171326, 82072072, 32261160372, 32371377,

82470532), the Leading Talent Project of Guangzhou Development District (2020-L013), the Guang Dong Basic and Applied Basic Research Foundation (2022B1515130010, 2021A1515111035), Natural Science Foundation of Guangdong Province (2022A1515011442), Dongguan Science and Technology of Social Development Program (20231800906311, 20221800906322).

Appendix A. Supplementary data

Supplementary data to this article can be found online at https://doi.org/10.1016/j.bioactmat.2024.09.011.

References

[1] R.N. Smith, J.P. Nolan, Central venous catheters, Br. Med. J. 347 (nov11 4) (2013) f6570, f6570.
[2] M. Zaccaria, M. Neri, F. Garzotto, C. Ronco, Principles of extracorporeal circulation and transport phenomena, in: C. Ronco, R. Bellomo, J.A. Kellum, Z. Ricci (Eds.), Critical Care Nephrology, Elsevier, Philadelphia, 2019, pp. 841–847.
[3] A. Guildford, M. Santin, G.J. Phillips, Cardiovascular stents, in: T. Gourlay, R. A. Black (Eds.), Biomaterials and Devices for the Circulatory System, Woodhead Publishing, 2010, pp. 173–216.
[4] I.H. Jaffer, J.C. Fredenburgh, J. Hirsh, J.I. Weitz, Medical device-induced thrombosis: what causes it and how can we prevent it? J. Thromb. Haemostasis 13 (S1) (2015) S72–S81.
[5] M. Gorbet, C. Sperling, M.F. Maitz, C.A. Siedlecki, C. Werner, M.V. Sefton, The blood compatibility challenge. Part 3: material associated activation of blood cascades and cells, Acta Biomater. 94 (2019) 25–32.
[6] I. Reviakine, F. Jung, S. Braune, J.L. Brash, R. Latour, M. Gorbet, W. van Oeveren, Stirred, shaken, or stagnant: what goes on at the blood–biomaterial interface, Blood Rev. 31 (1) (2017) 11–21.
[7] D. Campoccia, L. Montanaro, C.R. Arciola, A review of the biomaterials technologies for infection-resistant surfaces, Biomaterials 34 (34) (2013) 8533–8554.
[8] P. Lin, C.-W. Lin, R. Mansour, F. Gu, Improving biocompatibility by surface modification techniques on implantable bioelectronics, Biosens. Bioelectron. 47 (2013) 451–460.
[9] D. Zhang, Q. Chen, C. Shi, M. Chen, K. Ma, J. Wan, R. Liu, Dealing with the foreign-body response to implanted biomaterials: strategies and applications of new materials, Adv. Funct. Mater. 31 (6) (2020) 2007226.
[10] Y. Wo, E.J. Brisbois, R.H. Bartlett, M.E. Meyerhoff, Recent advances in thromboresistant and antimicrobial polymers for biomedical applications: just say yes to nitric oxide (NO), Biomater. Sci. 4 (8) (2016) 1161–1183.
[11] M.M. Bembea, G. Annich, P. Rycus, G. Oldenburg, I. Berkowitz, P. Pronovost, Variability in anticoagulation management of patients on extracorporeal membrane oxygenation, Pediatr. Crit. Care Med. 14 (2) (2013) e77–e84.
[12] K.G. Fischer, Essentials of anticoagulation in hemodialysis, Hemodial. Int. 11 (2) (2007) 178–189.
[13] G. Montalescot, D. Brieger, A.J. Dalby, S.-J. Park, R. Mehran, Duration of dual antiplatelet therapy after coronary stenting, J. Am. Coll. Cardiol. 66 (7) (2015) 832–847.
[14] L. Mauri, D.J. Kereiakes, R.W. Yeh, P. Driscoll-Shempp, D.E. Cutlip, P.G. Steg, S.-L. T. Normand, E. Braunwald, S.D. Wiviott, D.J. Cohen, D.R. Holmes, M.W. Krucoff, J. Hermiller, H.L. Dauerman, D.I. Simon, D.E. Kandzari, K.N. Garratt, D.P. Lee, T. K. Pow, P. Ver Lee, M.J. Rinaldi, J.M. Massaro, Twelve or 30 Months of dual antiplatelet therapy after drug-eluting stents, N. Engl. J. Med. 371 (23) (2014) 2155–2166.
[15] G.M. Arepally, Heparin-induced thrombocytopenia, Blood 129 (21) (2017) 2864–2872.
[16] M. Laine, F. Paganelli, L. Bonello, P2Y12-ADP receptor antagonists: days of future and past, World J. Cardiol. 8 (5) (2016) 327–332.
[17] S. Li, J.J.D. Henry, Nonthrombogenic approaches to cardiovascular bioengineering, Annu. Rev. Biomed. Eng. 13 (1) (2011) 451–475.
[18] D.C. Leslie, A. Waterhouse, J.B. Berthet, T.M. Valentin, A.L. Watters, A. Jain, P. Kim, B.D. Hatton, A. Nedder, K. Donovan, E.H. Super, C. Howell, C.P. Johnson, T.L. Vu, D.E. Bolgen, S. Rifai, A.R. Hansen, M. Aizenberg, M. Super, J. Aizenberg, D.E. Ingber, A bioinspired omniphobic surface coating on medical devices prevents thrombosis and biofouling, Nat. Biotechnol. 32 (11) (2014) 1134–1140.
[19] J. Zhang, X. Ke, M. Huang, X. Pei, S. Gao, D. Wu, J. Chen, Y. Weng, NO released via both a Cu-MOF-based donor and surface-catalyzed generation enhances anticoagulation and antibacterial surface effects, Biomater. Sci. 11 (1) (2023) 322–338.
[20] Y. Han, J. Yang, W. Zhao, H. Wang, Y. Sun, Y. Chen, J. Luo, L. Deng, X. Xu, W. Cui, H. Zhang, Biomimetic injectable hydrogel microspheres with enhanced lubrication and controllable drug release for the treatment of osteoarthritis, Bioact. Mater. 6 (10) (2021) 3596–3607.
[21] W. Wang, L. Lu, H.P. Bei, X. Li, Z. Du, M.F. Maitz, N. Huang, Q. Tu, X. Zhao, Z. Yang, Self-protonating, plasma polymerized, superimposed multi-layered biomolecule nanoreservoir as blood-contacting surfaces, Chem. Eng. J. 410 (2021) 128313.
[22] L. Li, C. Zhang, Z. Cao, L. Ma, C. Liu, X. Lan, C. Qu, P. Fu, R. Luo, Y. Wang, Passivation protein-adhesion platform promoting stent reendothelialization using two-electron-assisted oxidation of polyphenols, Biomaterials 305 (2024) 122423.
[23] X. Hu, J. Tian, C. Li, H. Su, R. Qin, Y. Wang, X. Cao, P. Yang, Amyloid-like protein aggregates: a new class of bioinspired materials merging an interfacial anchor with antifouling, Adv. Mater. 32 (23) (2020) e2000128.
[24] X. Mou, W. Miao, W. Zhang, W. Wang, Q. Ma, Z. Du, X. Li, N. Huang, Z. Yang, Zwitterionic polymers-armored amyloid-like protein surface combats thrombosis and biofouling, Bioact. Mater. 32 (2024) 37–51.
[25] Y.-N. Chou, A. Venault, C.-H. Cho, M.-C. Sin, L.-C. Yeh, J.-F. Jhong, A. Chinnathambi, Y. Chang, Y. Chang, Epoxylated zwitterionic triblock copolymers grafted onto metallic surfaces for general biofouling mitigation, Langmuir 33 (38) (2017) 9822–9835.
[26] S. Kim, Y. Jang, L.K. Jang, S.H. Sunwoo, T.-i. Kim, S.-W. Cho, J.Y. Lee, Electrochemical deposition of dopamine–hyaluronic acid conjugates for anti-biofouling bioelectrodes, J. Mater. Chem. B 5 (23) (2017) 4507–4513.
[27] N. Lyu, Z. Du, H. Qiu, P. Gao, Q. Yao, K. Xiong, Q. Tu, X. Li, B. Chen, M. Wang, G. Pan, N. Huang, Z. Yang, Mimicking the nitric oxide-releasing and glycocalyx functions of endothelium on vascular stent surfaces, Adv. Sci. 7 (21) (2020) 2002330.
[28] H. Qiu, P. Qi, J. Liu, Y. Yang, X. Tan, Y. Xiao, M.F. Maitz, N. Huang, Z. Yang, Biomimetic engineering endothelium-like coating on cardiovascular stent through heparin and nitric oxide-generating compound synergistic modification strategy, Biomaterials 207 (2019) 10–22.
[29] C. Li, D. Lu, J. Deng, X. Zhang, P. Yang, Amyloid-like rapid surface modification for antifouling and in-depth remineralization of dentine tubules to treat dental hypersensitivity, Adv. Mater. 31 (46) (2019) e1903973.
[30] F. Obstals, L. Witzdam, M. Garay-Sarmiento, N.Y. Kostina, J. Quandt, R. Rossaint, S. Singh, O. Grottke, C. Rodriguez-Emmenegger, Improving hemocompatibility: how can smart surfaces direct blood to fight against thrombi, ACS Appl. Mater. Interfaces 13 (10) (2021) 11696–11707.
[31] H. Wan, X. Yang, Y. Zhang, X. Liu, Y. Li, Y. Qin, H. Yan, L. Gui, K. Li, L. Zhang, L. Yang, B. Zhang, Y. Wang, Polyphenol-reinforced glycocalyx-like hydrogel coating induced myocardial regeneration and immunomodulation, ACS Nano 18 (32) (2024) 21512–21522.
[32] Z. Yang, X. Zhao, R. Hao, Q. Tu, X. Tian, Y. Xiao, K. Xiong, M. Wang, Y. Feng, N. Huang, G. Pan, Bioclickable and mussel adhesive peptide mimics for engineering vascular stent surfaces, Proc. Natl. Acad. Sci. USA 117 (28) (2020) 16127–16137.
[33] Y. Yang, P. Gao, J. Wang, Q. Tu, L. Bai, K. Xiong, H. Qiu, X. Zhao, M.F. Maitz, H. Wang, X. Li, Q. Zhao, Y. Xiao, N. Huang, Z. Yang, Endothelium-mimicking multifunctional coating modified cardiovascular stents via a stepwise metal-catechol-, Amine) Surface Engineering Strategy, Research 2020 (2020) 9203906.
[34] K. Li, J. Peng, Y. Liu, F. Zhang, D. Wu, R. Luo, Z. Du, L. Yang, G. Liu, Y. Wang, Surface engineering of central venous catheters via combination of antibacterial endothelium-mimicking function and fibrinolytic activity for combating blood stream infection and thrombosis, Adv. Healthcare Mater. 12 (23) (2023) e2300120.
[35] P. Li, W. Cai, K. Wang, L. Zhou, S. Tang, Y. Zhao, X. Li, J. Wang, Selenium-functionalized polycarbonate-polyurethane for sustained in situ generation of therapeutic gas for blood-contacting materials, Smart Mater. Med. 3 (2022) 361–373.
[36] Z. Du, F. Qiao, L. Tong, W. Zhang, X. Mou, X. Zhao, M.F. Maitz, H. Wang, N. Huang, Z. Yang, Mimicking Mytilus edulis foot protein: a versatile strategy for robust biomedical coatings, Innovation 5 (5) (2024) 100671.
[37] D. Li, H. Chen, J.L. Brash, Mimicking the fibrinolytic system on material surfaces, Colloids Surf., B 86 (1) (2011) 1–6.
[38] C. Li, H. Du, A. Yang, S. Jiang, Z. Li, D. Li, J.L. Brash, H. Chen, Thrombosis-responsive thrombolytic coating based on thrombin-degradable tissue plasminogen activator (t-PA) nanocapsules, Adv. Funct. Mater. 27 (45) (2017) 1703934.
[39] Y. Wang, H. Wu, Z. Zhou, M.F. Maitz, K. Liu, B. Zhang, L. Yang, R. Luo, Y. Wang, A thrombin-triggered self-regulating anticoagulant strategy combined with anti-inflammatory capacity for blood-contacting implants, Sci. Adv. 8 (9) (2022) eabm3378.
[40] D.G. Deutsch, E.T. Mertz, Plasminogen: purification from human plasma by affinity chromatography, Science 170 (3962) (1970) 1095–1096.
[41] W.G. McClung, D.L. Clapper, S.P. Hu, J.L. Brash, Adsorption of plasminogen from human plasma to lysine-containing surfaces, J. Biomed. Mater. Res. 49 (3) (2000) 409–414.
[42] N.A. Samoilova, M.A. Krayukhina, S.P. Novikova, T.A. Babushkina, I.O. Volkov, L. I. Komarova, L.I. Moukhametova, R.B. Aisina, E.A. Obraztsova, I.V. Yaminsky, I. A. Yamskov, Polyelectrolyte thromboresistant affinity coatings for modification of devices contacting blood, J. Biomed. Mater. Res., Part A 82A (3) (2007) 589–598.
[43] N.A. Samojlova, M.A. Krayukhina, I.A. Yamskov, Use of the affinity chromatography principle in creating new thromboresistant materials, J. Chromatogr. B 800 (1–2) (2004) 263–269.
[44] E. Anglés-Cano, Overview on fibrinolysis: plasminogen activation pathways on fibrin and cell surfaces, Chem. Phys. Lipids 67–68 (1994) 353–362.
[45] P. Libby, Inflammation in atherosclerosis, Arterioscler. Thromb. Vasc. Biol. 32 (9) (2012) 2045–2051.
[46] W. Zhan, X. Shi, Q. Yu, Z. Lyu, L. Cao, H. Du, Q. Liu, X. Wang, G. Chen, D. Li, J. L. Brash, H. Chen, Bioinspired blood compatible surface having combined fibrinolytic and vascular endothelium-like properties via a sequential coimmobilization strategy, Adv. Funct. Mater. 25 (32) (2015) 5206–5213.

[47] H. Gu, X. Chen, X. Liu, W. Zhan, Z. Lyu, Q. Yu, Z. Wu, H. Chen, A hemocompatible polyurethane surface having dual fibrinolytic and nitric oxide generating functions, J. Mater. Chem. B 5 (5) (2017) 980–987.
[48] H. Yu, H. Qiu, W. Ma, M.F. Maitz, Q. Tu, K. Xiong, J. Chen, N. Huang, Z. Yang, Endothelium-mimicking surface combats thrombosis and biofouling via synergistic long- and short-distance defense strategy, Small 17 (24) (2021) e2100729.
[49] Q. Ma, X. Shi, X. Tan, R. Wang, K. Xiong, M.F. Maitz, Y. Cui, Z. Hu, Q. Tu, N. Huang, L. Shen, Z. Yang, Durable endothelium-mimicking coating for surface bioengineering cardiovascular stents, Bioact. Mater. 6 (12) (2021) 4786–4800.
[50] M.F. Debets, S.S. van Berkel, J. Dommerholt, A.J. Dirks, F.P.J.T. Rutjes, F.L. van Delft, Bioconjugation with strained alkenes and alkynes, Acc. Chem. Res. 44 (9) (2011) 805–815.
[51] X. Mou, H. Zhang, H. Qiu, W. Zhang, Y. Wang, K. Xiong, N. Huang, H.A. Santos, Z. Yang, Mussel-inspired and bioclickable peptide engineered surface to combat thrombosis and infection, Research 2022 (2022) 9780879.
[52] Q. Tu, X. Shen, Y. Liu, Q. Zhang, X. Zhao, M.F. Maitz, T. Liu, H. Qiu, J. Wang, N. Huang, Z. Yang, A facile metal–phenolic–amine strategy for dual-functionalization of blood-contacting devices with antibacterial and anticoagulant properties, Mater. Chem. Front. 3 (2) (2019) 265–275.
[53] P. Gao, H. Qiu, K. Xiong, X. Li, Q. Tu, H. Wang, N. Lyu, X. Chen, N. Huang, Z. Yang, Metal-catechol-(amine) networks for surface synergistic catalytic modification: therapeutic gas generation and biomolecule grafting, Biomaterials 248 (2020) 119981.
[54] Y. Xiao, W. Wang, X. Tian, X. Tan, T. Yang, P. Gao, K. Xiong, Q. Tu, M. Wang, M. F. Maitz, N. Huang, G. Pan, Z. Yang, A versatile surface bioengineering strategy based on mussel-inspired and bioclickable peptide mimic, Research 2020 (2020) 7236946.
[55] J.W. Weisel, R.I. Litvinov, Mechanisms of fibrinolysis and basic principles of management, Hemostasis and Thrombosis (2014) 169–185.
[56] H. Xu, Y. Luan, Z. Wu, X. Li, Y. Yuan, X. Liu, L. Yuan, D. Li, H. Chen, Incorporation of lysine-containing copolymer with polyurethane affording biomaterial with specific adsorption of plasminogen, Chin. J. Chem. 32 (1) (2013) 44–50.
[57] Y. Ke, H. Meng, Z. Du, W. Zhang, Q. Ma, Y. Huang, L. Cui, Y. Lei, Z. Yang, Bioinspired super-hydrophilic zwitterionic polymer armor combats thrombosis and infection of vascular catheters, Bioact. Mater. 37 (2024) 493–504.
[58] W. Zhang, J. Zhang, F. Hu, W. Wang, Z. Du, Y. Ke, Q. Ma, X. Mou, J. Lu, Z. Yang, Active dual-protein coating assisted by stepwise protein–protein interactions assembly reduces thrombosis and infection, Adv. Sci. 11 (17) (2024) e2310259.